

MUSE Spectroscopic Identifications of Ultra-Faint Emission Line Galaxies with $M_{UV} \sim -15^*$

MICHAEL V. MASEDA,^{1,†} ROLAND BACON,² MARIJN FRANX,¹ JARLE BRINCHMANN,^{1,3} JOOP SCHAYE,¹ LEINDERT A. BOOGAARD,¹ NICOLAS BOUCHÉ,^{4,2}
RYCHARD J. BOUWENS,¹ SEBASTIANO CANTALUPO,⁵ THIERRY CONTINI,⁴ TAKUYA HASHIMOTO,^{6,7} HANAÉ INAMI,² RAFFAELLA A. MARINO,⁵
SOWGAT MUZAHID,¹ THEMIYA NANAYAKKARA,¹ JOHAN RICHARD,² KASPER B. SCHMIDT,⁸ ANNE VERHAMME,⁹ AND LUTZ WISOTZKI⁸

¹*Leiden Observatory, Leiden University, P.O. Box 9513, 2300 RA, Leiden, The Netherlands*

²*Univ Lyon, Univ Lyon1, Ens de Lyon, CNRS, Centre de Recherche Astrophysique de Lyon UMR5574, 69230, Saint-Genis-Laval, France*

³*Instituto de Astrofísica e Ciências do Espaço, Universidade do Porto, CAUP, Rua das Estrelas, PT4150-762 Porto, Portugal*

⁴*Institut de Recherche en Astrophysique et Planétologie (IRAP), Université de Toulouse, CNRS, UPS, F-31400 Toulouse, France*

⁵*ETH Zürich, Department of Physics, Wolfgang-Pauli-Str. 27, 8093 Zürich, Switzerland*

⁶*Department of Environmental Science and Technology, Faculty of Design Technology, Osaka Sangyo University, 3-1-1, Nagaito, Daito, Osaka 574-8530, Japan*

⁷*National Astronomical Observatory of Japan, 2-21-1 Osawa, Mitaka, Tokyo 181-8588, Japan*

⁸*Leibniz-Institut für Astrophysik Potsdam (AIP), An der Sternwarte 16, 14482 Potsdam, Germany*

⁹*Observatoire de Genève, Université de Genève, 51 Ch. des Maillettes, 1290 Versoix, Switzerland*

(Accepted August 29, 2018)

Submitted to The Astrophysical Journal Letters

ABSTRACT

Using an ultra-deep blind survey with the MUSE integral field spectrograph on the ESO Very Large Telescope, we obtain spectroscopic redshifts to a depth never explored before: galaxies with observed magnitudes $m_{AB} \geq 30 - 32$. Specifically, we detect objects via Lyman- α emission at $2.9 < z < 6.7$ without individual continuum counterparts in areas covered by the deepest optical/near-infrared imaging taken by the Hubble Space Telescope, the Hubble Ultra Deep Field. In total, we find 102 such objects in 9 square arcminutes at these redshifts. Detailed stacking analyses confirm the Lyman- α emission as well as the 1216 Å-breaks and faint UV continua ($M_{UV} \sim -15$). This makes them the faintest spectroscopically-confirmed objects at these redshifts, similar to the sources believed to reionize the universe. A simple model for the expected fraction of detected/undetected Lyman- α emitters as a function of luminosity is consistent with these objects being the high-equivalent width tail of the normal Lyman- α -emitter population at these redshifts.

Keywords: galaxies: high-redshift — galaxies: evolution

1. INTRODUCTION

Traditional spectroscopic studies rely on a pre-selection of objects, typically via photometry. Objects are selected based on a variety of criteria and are then targeted with slits or fibers that feed into a spectrograph. While this technique is widely used, it is nevertheless unreliable for obtaining complete spectroscopic samples whenever the input photometric

catalog is incomplete, e.g. when the objects of interest are near the detection limit of the imaging. This is particularly true when an emission line is the most significant contribution to the observed broadband magnitude, so objects with spectroscopically-detectable emission lines with high equivalent widths (EWs) might not be present in photometric catalogs (e.g. Figure 7 of Maseda et al. 2018).

Pure blind spectroscopic studies require exquisitely well-understood data to ensure reliable line detections and data from MUSE (the Multi-Unit Spectroscopic Explorer; Bacon et al. 2010), an Integral Field Spectrograph at the Very Large Telescope, are now in such a state. The recent survey of the Ultra Deep Field (UDF) with MUSE (Bacon et al. 2017, henceforth B17) reaches an unprecedented spectroscopic depth ($< 3 \times 10^{-19}$ erg s⁻¹ cm⁻² at 7000 Å; 3- σ for a spatially- and spectrally-unresolved line), with quality and

Corresponding author: Michael V. Maseda
maseda@strw.leidenuniv.nl

* Based on observations made with ESO telescopes at the La Silla Paranal Observatory under program IDs 094.A-2089(B), 095.A-0010(A), 096.A-0045(A), and 096.A-0045(B); and based on data obtained with the NASA/ESA *Hubble Space Telescope* which is operated by the Association of Universities for Research in Astronomy, Inc., under NASA contract NAS 5-26555.

† NOVA Fellow

uniformity that far exceeds the commissioning data in the Hubble Deep Field South (Bacon et al. 2015).

One result from B17, which is also hinted at in Bacon et al. (2015), is the presence of numerous emission line sources with no counterpart in catalogs based on Hubble Space Telescope (HST) imaging. While a fraction of these sources are not in photometric catalogs due to close blending issues, the remainder are plausibly extremely faint in the continuum ($m_{AB} \gtrsim 30$). They are believed to be HI Lyman- α emitters (LAEs) at redshifts $2.9 < z < 6.7$ due to an asymmetric line profile and/or the lack of other spectral features which would be indicative of lower- z sources. The implied ultraviolet (UV) magnitudes ($M_{UV} > -16$) are intriguing as galaxies this faint are thought to have reionized the universe at $z > 6$, but have so far remained elusive spectroscopically (e.g. Bouwens et al. 2012; Finkelstein et al. 2012). Detections of the UV continuum or other spectral features would provide further evidence that these “invisible” galaxies are indeed high- z LAEs.

In practice, deep non-detections of the UV continuum of an LAE implies that Lyman- α has a large EW. The interest in these LAEs is due to theoretical expectations where $EW_{Ly\alpha} \lesssim 200 \text{ \AA}$ if the photons are produced by normal stellar populations (Charlot & Fall 1993). This value can be exceeded at extremely low metallicities ($\lesssim 1\% Z_{\odot}$), young ages ($\lesssim 10 \text{ Myr}$), or with non-standard stellar initial mass functions, which are potential signatures of the earliest populations of galaxies in the universe (Schaerer 2003, Raiter et al. 2010; and also the discussion in Marino et al. 2018). While some narrow-band studies have explicitly attempted to constrain the fraction of high-EW LAEs (Malhotra & Rhoads 2002; Gronwall et al. 2007; Ouchi et al. 2008; Zheng et al. 2014), detailed spectroscopic and photometric studies have only confirmed this picture in a few cases (e.g. Kashikawa et al. 2012; Hashimoto et al. 2017a).

Here we present a sample of 102 LAEs detected by MUSE that are not significantly detected in the HST imaging in the UDF, which reaches depths of 29.1 – 30.3 (Illingworth et al. 2013). We use spectral stacking (Section 2.1) and photometric stacking (Section 3) to confirm the MUSE Lyman- α redshifts and estimate the contamination fraction. Finally, we demonstrate that the observed fraction of HST-undetected LAEs is in line with theoretical expectations (Section 4). We adopt a flat Λ CDM cosmology ($\Omega_m = 0.3$, $\Omega_{\Lambda} = 0.7$, and $H_0 = 70 \text{ km s}^{-1} \text{ Mpc}^{-1}$) and AB magnitudes (Oke 1974) throughout.

2. DATA AND SAMPLE SELECTION

We utilize the MUSE spectroscopic dataset in the UDF, covering 9.92 arcmin^2 to 10 hour depth and a single 1.15 arcmin^2 subfield to 32 hour depth: further details about the observations and data reduction are presented in B17.

The positioning of the MUSE data was designed to maximize the overlap with HST imaging in the UDF, the deepest imaging at UV, optical, and near-infrared wavelengths ever taken. Here, we utilize the reductions from Illingworth et al. (2013), who combine all epochs of imaging from all major surveys in the area (ACS $F435W$, $F606W$, $F775W$, and $F850LP$; WFC3/IR $F105W$, $F125W$, $F140W$, and $F160W$). We supplement these images with WFC3/UV $F225W$ data (Teplitz et al. 2013) and $F275W$ and $F336W$ data (Oesch et al. 2018).

We use the 160 sources from B17 with flux-weighted emission line centroids that cannot be attributed to photometric objects in the Rafelski et al. (2015, henceforth R15) catalog within $0'.6$ (the FWHM of MUSE; see Section 3.1 of Inami et al. 2017, henceforth I17). These sources were identified via a spatially- and spectrally-coherent emission line from the MUSE data using the ORIGIN software (Bourguignon et al. 2012; Paris 2013; B17; D. Mary et al. in prep.). As with the full I17 catalog, redshifts are determined via template cross-correlation and human inspection. Combined with the fact that Lyman- α is spectrally-resolved in MUSE, this means that a majority of the LAEs have fluxes far above the nominal $3\text{-}\sigma$ limit (see Figure 1 and Table 1).

2.1. Detected versus Undetected

With this sample of 160 objects that are not in the R15 catalog, we proceed to measure the magnitudes in order to exclude all HST-detected objects. We utilize the signal-to-noise (S/N) ratio in HST images within a $0'.4$ aperture centered on the Lyman- α centroid from ORIGIN. This aperture corresponds to a physical size of 3.1 kpc (2.2 kpc) at $z = 2.9$ (6.6). However, as shown in Section 3, stacked images show that the objects are, on average, more compact than this aperture (and in agreement with measured size-luminosity relations, e.g. Shibuya et al. 2015).

The local background level is calculated by measuring the standard deviation of the fluxes in 250 identical apertures spread randomly within a $10'' \times 10''$ cutout centered on the object, with other objects masked according to the R15 segmentation maps. Because the UDF is not uniform in all photometric bands (specifically the WFC3 coverage), it is crucial to measure the *local* background level instead of relying on the average depth of the field. If the aperture flux is greater than five times the local background level in an HST band, then we consider the object “detected” in that band.

In total, we find that 102 of the ORIGIN sources are not detected above $5\text{-}\sigma$ in any of the HST imaging bands, all of which have redshifts classified as Lyman- α (I17). This represents 12.6% of the full I17 LAE sample. At $z > 6$ where an LAE has most of its flux redwards of $F850LP$, we only have a single object that lies outside of the deepest WFC3/IR data in the UDF.

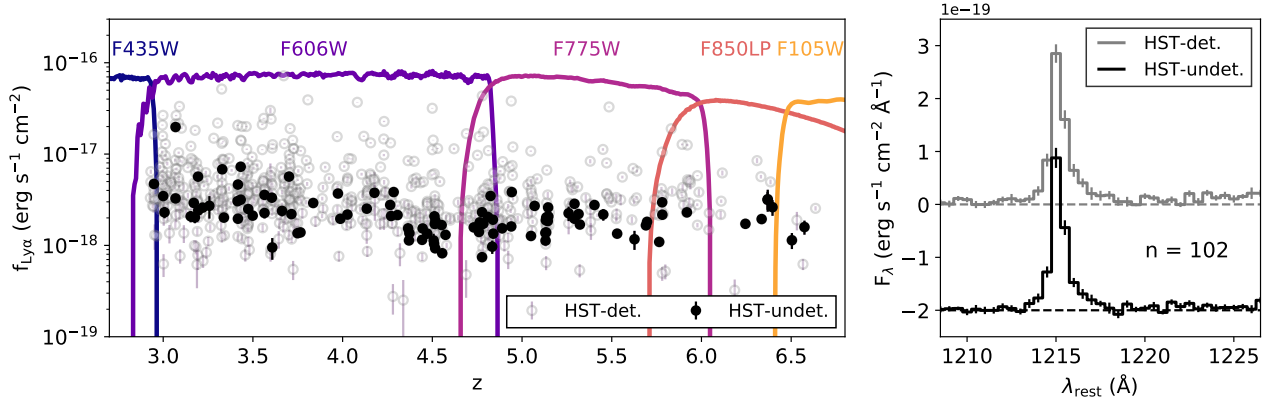


Figure 1. (Left) $f_{Ly\alpha}$ versus z for the HST-undetected (filled circles) and HST-detected MUSE LAEs (open circles), with HST imaging filter curves denoted by solid lines. (Right) MUSE spectral stacks (median; bootstrap uncertainties) of LAEs. The black spectrum shows the HST-undetected LAEs (offset by -2) and the gray spectrum is a flux- and redshift-matched sample of 102 HST-detected LAEs. Lyman- α is clearly detected with good agreement between the HST-detected/undetected LAEs, including the characteristic asymmetry of Lyman- α .

Their Lyman- α fluxes and redshifts compared to the full MUSE sample of HST-detected LAEs are shown in the left panel of Figure 1. Compared to a Lyman- α flux- and redshift-matched sample of HST-detected MUSE LAEs, we see a similar Lyman- α amplitude and spectral profile (right panel of Figure 1; see I17 for details on the spectral extractions), confirming the reality of the ORIGIN line detections. The MUSE “HST-undetected” sample is presented in Table 1. The median aperture S/N in *F606W* of our sample is 1.0, compared with 9.9 for the 663 MUSE-confirmed LAEs that are in the R15 catalog.

Of the 58 ORIGIN-only LAEs with an HST detection, 11 are detected only in the photometric band(s) that contains Lyman- α . While they are omitted from this sample, they are also plausibly high-EW LAEs since their UV continuum is still undetected (Maseda et al. in prep.). The remaining sources are not in the R15 catalog primarily because of their projected proximity to brighter galaxies (B17). Our sample is clearly separated from the HST-detected R15 sources at these redshifts, even though our aperture measurements often represent lower limits to the actual magnitudes (Figure 2).

3. HST IMAGING STACKS

We create stacks in each imaging band, adopting three redshift bins ($2.974 < z < 4.646$, $4.877 < z < 5.678$, and $6.067 < z < 6.389$) spaced such that the Lyman- α flux lies in a single HST band (*F606W*, *F775W*, and *F850LP*, respectively; see Figure 1). These bins contain 54, 22, and 4 objects.

In each bin we combine the HST imaging for all objects on a filter-by-filter basis. In each filter stack, we take the mean flux value at each pixel position, using the R15 segmentation maps to mask other sources. These stacks are shown in Figure 3, restricting the view to the band containing

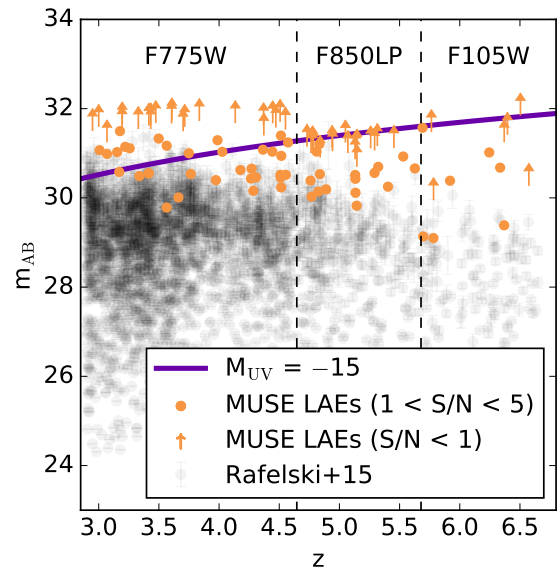


Figure 2. Redshift versus observed magnitude for the 102 MUSE HST-undetected LAEs and the photometric sample of R15. Magnitudes are given in the band immediately redwards of Lyman- α ; for the MUSE objects, the measurement is within a $0''.4$ aperture, with circles showing measurements ($S/N < 5$) and arrows showing the $1-\sigma$ noise level in the aperture when $S/N < 1$. The R15 redshifts are photometric whereas the MUSE redshifts are spectroscopic. A line of constant $M_{UV} = -15$ is shown in purple, similar to the values from stacks presented in Section 3. The MUSE sample is, by construction, much fainter than the R15 sample.

Lyman- α and the bands immediately redwards/bluewards. The UV continuum appears compact compared to the photometric aperture and therefore we conclude that a majority of our sample have small sizes ($r_e \lesssim 1.5$ kpc). In addition, when combining all filters redwards of Lyman- α for *individ-*

ual galaxies, 18 have a detection of their UV continuum. In these cases we do not measure a significant offset between the centroid of Lyman- α and the UV continuum (median $0''.09$, equal to the size of the HST/ACS point spread function; cf. Finkelstein et al. 2011; Sobral et al. 2017).

We perform aperture photometry on the stacks in the same way as described in Section 2.1. The UV continuum magnitudes, in the band redwards of Lyman- α , for the two lower- z bins are -14.67 and -15.36 , and -15.37 ($1-\sigma$) for the highest- z bin, at the median redshifts within the bins.

The effect of Lyman- α on the two lower- z stacks is clear, resulting in strong detections in those bands. While undetected individually in *F850LP* and *F105W*, the high- z stack of 4 objects has a significance of $3.0-\sigma$ when the two filters are combined. The lack of detections in the blue bands indicates a drop in the spectral energy distribution, likely from the 1216 \AA -break, further demonstrated by the fact that these stacks satisfy the color selections for “dropout” galaxies from Bouwens et al. (2015). This all implies that the average galaxy in our sample is indeed at the redshift expected based on the position and identification of Lyman- α .

If we were to use only the faintest objects in the sample (i.e. $S/N < 3$ in all HST bands), then we would have stacks of 30, 11, and 4 objects resulting in M_{UV} values of -14.07 , -15.29 , and -15.37 , also satisfying the “dropout” color selections.

3.1. Fraction of Interlopers

The primary source of contamination in our ORIGIN sample are emission lines being misidentified as Lyman- α . Lyman- α is often but not always identified via its characteristic asymmetry, otherwise a single emission feature is identified as Lyman- α when no other emission/absorption features can be detected in the spectrum. [O II] would be the primary line that is misidentified as Lyman- α considering that other strong optical emission lines ($H\alpha$, [O III], or $H\beta$) are almost never observed alone at MUSE wavelengths and [O II] is the only strong emission line observable at $0.9 < z < 1.5$. We expect misidentifications predominantly at low S/N , as the spectral resolution of MUSE is high enough to differentiate the two peaks of the [O II] doublet ($\approx 200 \text{ km s}^{-1}$) from the typical separation of double-peaked $z \approx 3 - 6$ LAEs ($\approx 500 \text{ km s}^{-1}$; Trainor et al. 2015; Verhamme et al. 2018).

In order to assess the potential contamination fraction we recreate the HST imaging stacks shown in Figure 3, randomly replacing a number of the (plausible) LAEs, n , with MUSE-confirmed [O II] emitters with a similar line flux and line position. For these “contaminated” samples with varying n we perform the same stacking procedure, measuring the S/N in the band bluewards of (the misidentified) Lyman- α (*F435W*, *F606W*, and *F775W*, respectively) which is critical in identifying the 1216 \AA -break. This procedure is repeated 1000 times (replacing a random subset of n objects with [O

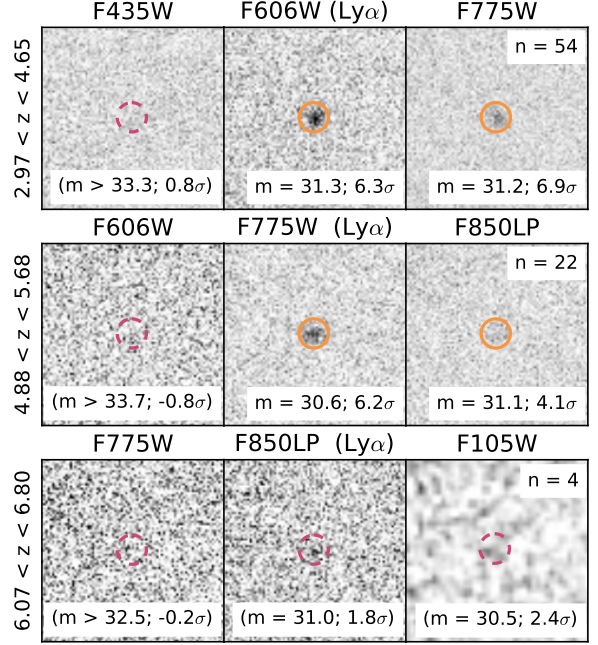


Figure 3. HST image stacks for the HST-undetected LAEs, separated into redshift bins. Each image is $2''.5$ on a side; the solid (dashed) circle shows a $0''.4$ aperture with $>3-\sigma$ detections (non-detections) in orange (pink). The 1216 \AA -break is demonstrated by non-detections in the left panels as well as Lyman- α emission and the UV continuum in the central/right panels, providing photometric proof that the average object is a high- z LAE. Numbers of objects per stack, magnitudes ($1-\sigma$ limits when $S/N < 1$), and detection significances are also shown.

II] emitters each time) to measure the fraction of cases where the stacks are detected at $> 3-\sigma$. For these stacks, $n \geq 3$, 1, and 1 produces detections in the blue band $> 99.7\%$ of the time, implying contamination fractions of $< 6\%$, $< 5\%$, and $< 25\%$, respectively.

4. COMPARISON TO CONTINUUM-DETECTED SAMPLES

In order to assess if the HST-undetected objects are a separate population or an extension of the HST-detected population, we construct an empirical model based on a distribution of rest-frame Lyman- α EWs and a distribution of UV continuum magnitudes. We use the observed EW distribution for HST-detected MUSE LAEs in the UDF (Hashimoto et al. 2017b), assuming no evolution in this distribution with redshift or $L_{Ly\alpha}$ (see their Section 6.3). The best-fit lognormal distribution has a mean EW of 119 \AA (15% of objects have EWs in excess of 200 \AA). We model the distribution of M_{UV} values as a power-law with α -slopes from Bouwens et al. (2015) at $z \sim 4, 5$, and 6.

By combining these distributions, we can predict the number of objects with a given M_{UV} and $EW_{Ly\alpha}$. These two

parameters determine the number of objects that would be spectroscopically-detectable by MUSE with total luminosities (line plus continuum) that would have been observed at the average depth of the HST imaging: 30.1 in $F606W$, 30.1 in $F775W$, and 29.2 in $F850LP$, depending on the redshift (Illingworth et al. 2013), and including the mean attenuation of the intergalactic medium (Inoue et al. 2014). This model can be inverted for a given $L_{\text{Ly}\alpha}$ to give the number of sources above the HST limits (for the assumed EW distribution). We use larger redshift ranges ($2.9 < z < 4.88$, $4.88 < z < 6.07$, and $6.07 < z < 6.65$) than in Section 3 since contribution of Lyman- α to a bluer/redder HST band is not important. The resulting predictions for the undetected fraction as a function of $L_{\text{Ly}\alpha}$ are shown in Figure 4, using the observed redshift distribution of the MUSE HST-undetected sources. Overplotted is the fraction of HST-detected/undetected sources from MUSE.

Overall this model accurately reproduces the observed fractions: comparing the distributions of $L_{\text{Ly}\alpha}$, we obtain p -values from a Kolmogorov-Smirnov test of 0.07, 0.68, and 0.97. While this does not imply with certainty that this is the *best* model to explain the observations, it means that the HST-undetected LAEs are consistent with being the (high-EW) tail of the distribution of HST-detected LAEs.

A natural question is whether the phenomenon of a MUSE line detection without an HST counterpart occurs for emission lines other than Lyman- α . For example, there are no cases where ORIGIN detects [O II] emission without an HST counterpart. We can perform a similar analysis to the one above to see if this matches expectations. We adopt the [O II] luminosity function from Pirzkal et al. (2013), measured from HST/ACS slitless grism spectroscopy with coverage of [O II] from $0.9 < z < 1.5$, which is the high- z range probed by MUSE. At the luminosities probed by MUSE, this function can be approximated by a power law with a slope $\alpha = -1.93$. This is combined with the EW distribution from Pirzkal et al. (2013) (or I17) to estimate the continuum levels. We predict that the incidence of HST-undetected [O II] emission is essentially zero for $L_{[\text{O II}]} > 10^{39.5} \text{ erg s}^{-1}$ ($6 \times 10^{-19} \text{ erg s}^{-1} \text{ cm}^{-2}$ at $z = 1$). Only at $m_{F606W} = 29.2$ (0.9 magnitudes brighter than our data) would we expect 10% of $z = 1$ [O II] emitters at this luminosity to remain undetected in the continuum.

5. DISCUSSION AND CONCLUSIONS

We have discussed a sample of 102 emission line sources discovered with ultra-deep MUSE spectroscopy in the UDF. While they are all individually below the detection limits in HST-based imaging, stacks show flux distributions that are expected if these emission lines are predominantly Lyman- α . Notably, a strong detection in the HST bands expected to contain Lyman- α and the UV continuum from the two well-

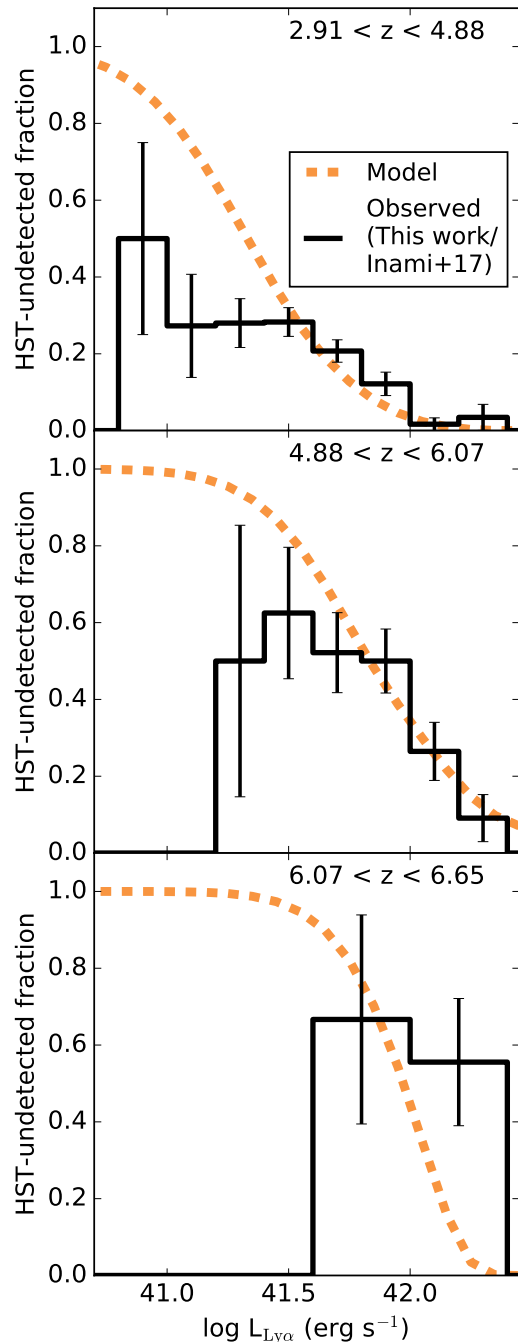


Figure 4. Observed (histogram; Poisson errors) and predicted (dashed line) fraction of LAEs in a MUSE-selected sample ($f_{\text{Ly}\alpha} > 3 \times 10^{-19} \text{ erg s}^{-1} \text{ cm}^{-2}$) that are undetected in broadband imaging at the depth of the UDF. The model is based on UV luminosity functions (Bouwens et al. 2015) and a Lyman- α EW distribution (Hashimoto et al. 2017b). Using the observed redshift distribution of undetected sources, the model predicts the dashed curve. Without any additional tuning we observe good agreement between the prediction and the observed fractions at all redshifts, implying that the HST-detected and undetected objects follow similar trends in UV magnitude and rest-frame Lyman- α EW.

populated stacks at $2.974 < z < 4.646$ and $4.877 < z < 5.678$, and in stacked MUSE spectra, implies that the ORIGIN line detections are robust. A detection in the combined Lyman- α and UV-continuum image in the $6.067 < z < 6.389$ bin also hints at the same conclusion. We have quantified the amount of contamination from [O II] emission lines that are misidentified as Lyman- α and find that the observed spectral break would disappear for contamination fractions as low as 5%. Finally, a simple model utilizing UV luminosity functions and an empirical Lyman- α EW distribution can reproduce the observed fraction of HST-undetected LAEs in our MUSE sample, implying that these sources are consistent with being an extension of the general population of LAEs.

Our stacking experiment reveals $M_{UV} \sim -15$ for these LAEs, or even -14 for the faintest subset. Compared to spectroscopically-confirmed narrow-band LAEs (e.g. Ouchi et al. 2008; Kashikawa et al. 2011; Zheng et al. 2014, $M_{UV} \lesssim -17.5$), Lyman-break galaxies (e.g. Stark et al. 2010, $M_{UV} \lesssim -18$), or MUSE LAEs in the UDF with HST counterparts (Hashimoto et al. 2017b, $M_{UV} \lesssim -16$), this sample is considerably fainter and represents the faintest objects at these redshifts with spectroscopic confirmations. These magnitudes are comparable to those of local blue compact dwarfs such as I Zw 18 ($M_{UV} = -14.7$; Gil de Paz et al. 2007). An abundant population of galaxies with such faint magnitudes at $z > 6$ are thought to be required in order to reionize the universe (Bouwens et al. 2012; Finkelstein et al. 2012), yet even our highly sensitive observations confirm $< 1\%$ of the expected numbers at $5 < z < 6.7$ with $-16 < M_{UV} < -14$ based on the $z \sim 6$ luminosity function (Bouwens et al. 2015), presumably those with the highest-EWs.

The ability to find emission lines in such faint sources crucially hinges on both the depth of the imaging data (to con-

firm the faint continua) as well as the depth of the spectroscopic data (these MUSE data probe line fluxes up to $10\times$ fainter than narrow-band studies at similar redshifts: Karman et al. 2017; Drake et al. 2017; Hashimoto et al. 2017b), which is unique to the MUSE UDF Survey. The next step is to properly characterize the physical properties of this unique population. By pushing towards LAEs with higher EWs, we can push towards the lowest ages (and hence masses) and metallicities. While this is challenging with traditional studies (Hashimoto et al. 2017a), we can perform robust statistical measurements using the MUSE spectroscopic sample due to the stringent constraints provided by the HST imaging.

We would like to thank the anonymous referee for useful comments that have improved the quality of the manuscript. RB acknowledges support from ERC grant 339659-MUSICOS. JB is supported through Investigador FCT contract IF/01654/2014/CP1215/CT0003, national funds (UID/FIS/04434/2013), and by FEDER through COMPETE2020 (POCI-01-0145-FEDER-007672). JS acknowledges support from ERC grant 278594-GasAroundGalaxies. SC acknowledges support from Swiss National Science Foundation grant PP00P2_163824. TC and NB acknowledge support from ANR FOGHAR (ANR-13-BS05-0010-02), OCEVU Labex (ANR-11-LABX-0060), and the A*MIDEX project (ANR-11-IDEX-0001-02) funded by the ‘‘Investissements d’avenir’’ program managed by the ANR. JR acknowledges support from ERC grant 336736-CALENDS. AV acknowledges support from ERC grant 757258-TRIPLE.

Table 1. Properties of HST-undetected MUSE LAEs. (abridged)

MUSE ID	RA	Dec	z	Ly α Flux	log Ly α Luminosity	S/N F_{435W}	S/N F_{606W}	S/N F_{775W}
(I17)	(deg)	(deg)		($\times 10^{-20}$ erg s $^{-1}$ cm $^{-2}$)	(erg s $^{-1}$)			
6316	53.17032	-27.77835	4.446	153. \pm 7.94	41.48 \pm 0.02251	-1.1	-0.34	-1.0
6317	53.16767	-27.77743	5.404	277. \pm 13.6	41.94 \pm 0.02140	0.23	0.58	4.2
6318	53.16665	-27.77651	4.555	82.1 \pm 7.49	41.23 \pm 0.03963	-0.29	0.022	2.9
6320	53.16465	-27.78574	4.516	92.9 \pm 8.20	41.28 \pm 0.03831	-0.0024	1.6	3.6
6321	53.16334	-27.78037	3.765	139. \pm 13.1	41.27 \pm 0.04095	0.0049	2.7	2.7

NOTE—The unabridged table (102 entries) can be found in the electronic version of the Journal.

REFERENCES

- Bacon, R., Accardo, M., Adjali, L., et al. 2010, in Proc. SPIE, Vol. 7735, Ground-based and Airborne Instrumentation for Astronomy III, 773508
- Bacon, R., Brinchmann, J., Richard, J., et al. 2015, *A&A*, 575, A75, doi: [10.1051/0004-6361/201425419](https://doi.org/10.1051/0004-6361/201425419)
- Bacon, R., Conseil, S., Mary, D., et al. 2017, *A&A*, 608, A1, doi: [10.1051/0004-6361/201730833](https://doi.org/10.1051/0004-6361/201730833)
- Bourguignon, S., Mary, D., & Slezak, E. 2012, *Statistical Methodology*, 9, 32, doi: <http://dx.doi.org/10.1016/j.stamet.2011.04.010>
- Bouwens, R. J., Illingworth, G. D., Oesch, P. A., et al. 2012, *ApJL*, 752, L5, doi: [10.1088/2041-8205/752/1/L5](https://doi.org/10.1088/2041-8205/752/1/L5)
- . 2015, *ApJ*, 803, 34, doi: [10.1088/0004-637X/803/1/34](https://doi.org/10.1088/0004-637X/803/1/34)
- Charlot, S., & Fall, S. M. 1993, *ApJ*, 415, 580, doi: [10.1086/173187](https://doi.org/10.1086/173187)
- Drake, A. B., Garel, T., Wisotzki, L., et al. 2017, *A&A*, 608, A6, doi: [10.1051/0004-6361/201731431](https://doi.org/10.1051/0004-6361/201731431)
- Finkelstein, S. L., Cohen, S. H., Windhorst, R. A., et al. 2011, *ApJ*, 735, 5, doi: [10.1088/0004-637X/735/1/5](https://doi.org/10.1088/0004-637X/735/1/5)
- Finkelstein, S. L., Papovich, C., Ryan, R. E., et al. 2012, *ApJ*, 758, 93, doi: [10.1088/0004-637X/758/2/93](https://doi.org/10.1088/0004-637X/758/2/93)
- Gil de Paz, A., Boissier, S., Madore, B. F., et al. 2007, *The Astrophysical Journal Supplement Series*, 173, 185, doi: [10.1086/516636](https://doi.org/10.1086/516636)
- Gronwall, C., Ciardullo, R., Hickey, T., et al. 2007, *ApJ*, 667, 79, doi: [10.1086/520324](https://doi.org/10.1086/520324)
- Hashimoto, T., Ouchi, M., Shimasaku, K., et al. 2017a, *MNRAS*, 465, 1543, doi: [10.1093/mnras/stw2834](https://doi.org/10.1093/mnras/stw2834)
- Hashimoto, T., Garel, T., Guiderdoni, B., et al. 2017b, *A&A*, 608, A10, doi: [10.1051/0004-6361/201731579](https://doi.org/10.1051/0004-6361/201731579)
- Illingworth, G. D., Magee, D., Oesch, P. A., et al. 2013, *ApJS*, 209, 6, doi: [10.1088/0067-0049/209/1/6](https://doi.org/10.1088/0067-0049/209/1/6)
- Inami, H., Bacon, R., Brinchmann, J., et al. 2017, *A&A*, 608, A2, doi: [10.1051/0004-6361/201731195](https://doi.org/10.1051/0004-6361/201731195)
- Inoue, A. K., Shimizu, I., Iwata, I., & Tanaka, M. 2014, *MNRAS*, 442, 1805, doi: [10.1093/mnras/stu936](https://doi.org/10.1093/mnras/stu936)
- Karman, W., Caputi, K. I., Caminha, G. B., et al. 2017, *A&A*, 599, A28, doi: [10.1051/0004-6361/201629055](https://doi.org/10.1051/0004-6361/201629055)
- Kashikawa, N., Shimasaku, K., Matsuda, Y., et al. 2011, *ApJ*, 734, 119, doi: [10.1088/0004-637X/734/2/119](https://doi.org/10.1088/0004-637X/734/2/119)
- Kashikawa, N., Nagao, T., Toshikawa, J., et al. 2012, *ApJ*, 761, 85, doi: [10.1088/0004-637X/761/2/85](https://doi.org/10.1088/0004-637X/761/2/85)
- Malhotra, S., & Rhoads, J. E. 2002, *ApJL*, 565, L71, doi: [10.1086/338980](https://doi.org/10.1086/338980)
- Marino, R. A., Cantalupo, S., Lilly, S. J., et al. 2018, *ApJ*, 859, 53, doi: [10.3847/1538-4357/aab6aa](https://doi.org/10.3847/1538-4357/aab6aa)
- Maseda, M. V., van der Wel, A., Rix, H.-W., et al. 2018, *ApJ*, 854, 29, doi: [10.3847/1538-4357/aaa76e](https://doi.org/10.3847/1538-4357/aaa76e)
- Oesch, P. A., Montes, M., Reddy, N., et al. 2018, *ApJS*, 237, 12, doi: [10.3847/1538-4365/aacb30](https://doi.org/10.3847/1538-4365/aacb30)
- Oke, J. B. 1974, *ApJS*, 27, 21, doi: [10.1086/190287](https://doi.org/10.1086/190287)
- Ouchi, M., Shimasaku, K., Akiyama, M., et al. 2008, *ApJS*, 176, 301, doi: [10.1086/527673](https://doi.org/10.1086/527673)
- Paris, S. 2013, *Theses*, Université Nice Sophia Antipolis; Università degli studi La Sapienza (Rome). <https://tel.archives-ouvertes.fr/tel-00933827>
- Pirzkal, N., Rothberg, B., Ly, C., et al. 2013, *ApJ*, 772, 48, doi: [10.1088/0004-637X/772/1/48](https://doi.org/10.1088/0004-637X/772/1/48)
- Rafelski, M., Teplitz, H. I., Gardner, J. P., et al. 2015, *AJ*, 150, 31, doi: [10.1088/0004-6256/150/1/31](https://doi.org/10.1088/0004-6256/150/1/31)
- Raiter, A., Schaerer, D., & Fosbury, R. A. E. 2010, *A&A*, 523, A64, doi: [10.1051/0004-6361/201015236](https://doi.org/10.1051/0004-6361/201015236)
- Schaerer, D. 2003, *A&A*, 397, 527, doi: [10.1051/0004-6361:20021525](https://doi.org/10.1051/0004-6361:20021525)
- Shibuya, T., Ouchi, M., & Harikane, Y. 2015, *ApJS*, 219, 15, doi: [10.1088/0067-0049/219/2/15](https://doi.org/10.1088/0067-0049/219/2/15)
- Sobral, D., Matthee, J., Best, P., et al. 2017, *MNRAS*, 466, 1242, doi: [10.1093/mnras/stw3090](https://doi.org/10.1093/mnras/stw3090)
- Stark, D. P., Ellis, R. S., Chiu, K., Ouchi, M., & Bunker, A. 2010, *MNRAS*, 408, 1628, doi: [10.1111/j.1365-2966.2010.17227.x](https://doi.org/10.1111/j.1365-2966.2010.17227.x)
- Teplitz, H. I., Rafelski, M., Kurczynski, P., et al. 2013, *AJ*, 146, 159, doi: [10.1088/0004-6256/146/6/159](https://doi.org/10.1088/0004-6256/146/6/159)
- Trainor, R. F., Steidel, C. C., Strom, A. L., & Rudie, G. C. 2015, *ApJ*, 809, 89, doi: [10.1088/0004-637X/809/1/89](https://doi.org/10.1088/0004-637X/809/1/89)
- Verhamme, A., Garel, T., Ventou, E., et al. 2018, *MNRAS*, 478, L60, doi: [10.1093/mnras/sly058](https://doi.org/10.1093/mnras/sly058)
- Zheng, Z.-Y., Wang, J.-X., Malhotra, S., et al. 2014, *MNRAS*, 439, 1101, doi: [10.1093/mnras/stu054](https://doi.org/10.1093/mnras/stu054)